NANO LETTERS

Letter

pubs.acs.org/NanoLett

Rainbow Radiating Single-Crystal Ag Nanowire Nanoantenna

Taejoon Kang,[†] Wonjun Choi,[∥] Ilsun Yoon,[†] Hyoban Lee,[†] Min-Kyo Seo,*[,‡,§] Q-Han Park,*[,∥] and Bongsoo Kim*[,†,§]

[†]Department of Chemistry, [‡]Department of Physics, and [§]KAIST Institute for the NanoCentury, KAIST, Daejeon 305-701, Korea
[∥]Department of Physics, Korea University, Seoul 136-701, Korea

Supporting Information

ABSTRACT: Optical antennas interface an object with optical radiation and boost the absorption and emission of light by the objects through the antenna modes. It has been much desired to enhance both excitation and emission processes of the quantum emitters as well as to interface multiwavelength channels for many nano-optical applications. Here we report the experimental implementation of an optical antenna operating in the full visible range via surface plasmon currents induced in a defect-free single-crystalline Ag nanowire (NW). With its atomically flat surface, the long Ag NW reliably establishes multiple plasmonic resonances and produces a unique rainbow antenna radiation in the Fresnel region. Detailed antenna radiation properties, such as radiating near-field patterns and polarization states, were experimentally examined and precisely analyzed by numerical simulations and antenna theory. The multiresonant Ag NW nanoantenna will find superb applications in nano-optical spectroscopy, high-resolution nanoimaging, photovoltaics, and nonlinear signal conversion.

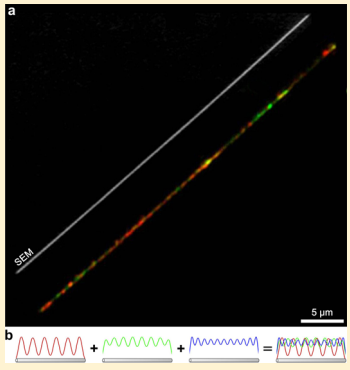

KEYWORDS: *Antenna, nanowires, silver, single-crystal, surface plasmon polariton*

Optical antennas, as a miniaturization of radio antenna, which convert freely propagating optical radiation into localized fields and vice versa, have contributed significantly to exploring key questions in the fields of nanosciences.[1−8] In particular, plasmonic nanoantennas can engineer confinement and absorption of light into specific targets of a nanosize and control emission properties and even transition lifetimes of fluorescent molecules or photoluminescent quantum dots interfaced with the antenna.[8−16]

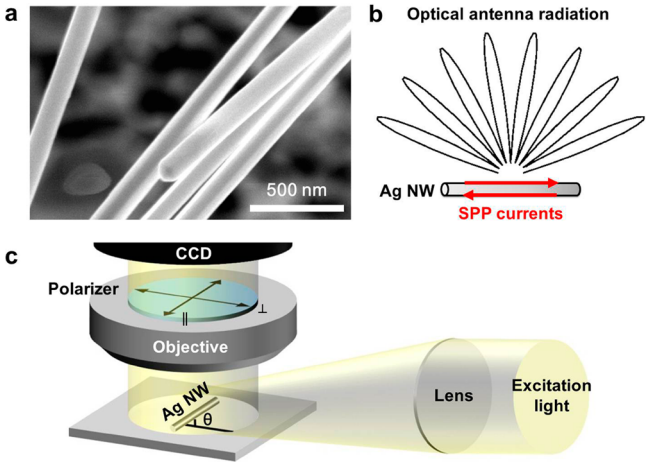

Figure 1. (a) SEM image of single-crystalline Ag NWs synthesized by vapor transport method. As-grown Ag NWs have atomically smooth surfaces. (b) Schematic of single Ag NW SPP antenna radiation. Ag NW that has an ultrasmooth surface can support charge-density waves, SPP currents, reflected at both ends of the NW. This alternating current in a Ag NW generates a typical multilobe radiation pattern in the free space, as illustrated. (c) Schematic of the measurement setup for Ag NW SPP antenna radiation in the Fresnel region.

Typical plasmonic nanoantennas, however, employing small metallic nanostructures such as a bow-tie or nanoparticles have only a single resonance with a finite spectral width.[5,11−14,16] For optimum interface with the radiation field, nanoantennas often need to play a dual role as a receiver and a transmitter at the same time, for which the operating frequencies can be different.[2,3,7] Furthermore, multiwavelength channels are frequently required in broadband nano-optical spectroscopy[17−20] as well as in biochemical sensing employing multiple emitters operating at different colors.[21−25] In this regard, development of plasmonic nanoantennas reliably operating at multiple resonances in the full visible range is a challenging but much desired task.[2,3,6−8]

Because silver has no interband electronic transition at visible wavelengths[26] and a sufficiently long metal nanowire (NW) can support multiple surface plasmon polariton (SPP) resonances in a wide spectral range,[27−32] a Ag NW could become a superb candidate for the plasmonic nanoantenna, which can transmit and receive optical signals at multiple wavelengths. A critical problem has yet to be solved to control the Ag NW antenna operation as desired. Multiple SPP resonances in a Ag NW require long distance propagation of SPP along the NW surface

Received: January 19, 2012
Revised: March 27, 2012
Published: April 11, 2012

   dx.doi.org/10.1021/nl3002414 | *Nano Lett.* 2012, 12, 2331−2336

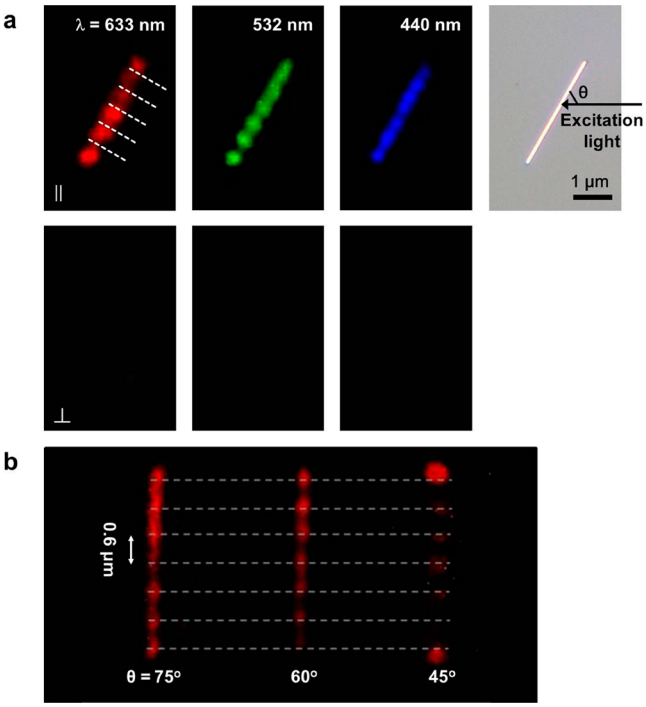

Figure 2. (a) SPP antenna radiating near-field patterns excited by 633 (red), 532 (green), and 440 nm (blue) lasers, respectively. The right panel shows an optical microscope image of the Ag NW nanoantenna. The Ag NW has a length of 3.1 μm and a diameter of 150 nm. The three figures at the top are radiation patterns when we detect only the light polarized parallel to the NW, and the three figures at the bottom perpendicular. The antenna radiations are strongly polarized along the NW axis. The white dashed lines superposed onto the pattern of 633 nm are corresponding to the lines represented in the simulation result of 630 nm in Figure 4a. (b) Ag NW antenna radiation patterns observed by 633 nm laser at different incident angles (75, 60, and 45°) with respect to the NW axis. The positions of the lobes are independent of the incident angle of the excitation laser, θ.

for many round trips, and thus the antenna surface should have extreme smoothness to avoid scattering of SPP, not obtainable by top-down techniques such as focused ion beam or electron-beam lithography.

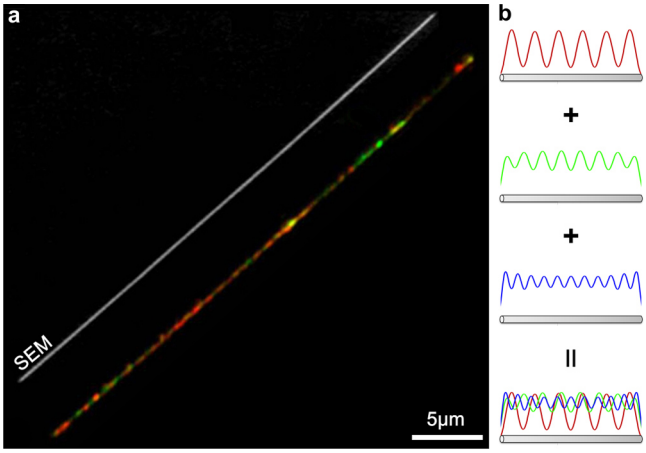

Figure 3. (a) Exitation of multiple resonances by white light generates a rainbow-like colorful radiation pattern. (b) Schematic illustration of rainbow radiating near-field pattern originated from multiple SPP antenna resonances at different wavelengths.

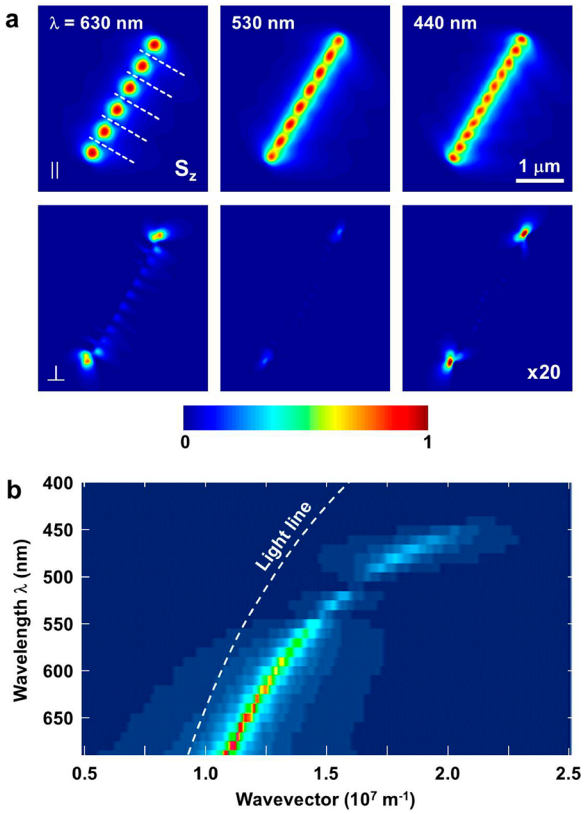

Figure 4. (a) Simulated results for vertical components of the Poynting vector of antenna radiations at three wavelengths calculated by the FDTD method at 150 nm above the NW axis. The white dashed lines in the pattern of 630 nm indicate the positions of the radiation nodes in Figure 2a. The observed and simulated results match very well. Experimental profiles in Figure 2a are blurred due to the numerical aperture of the objective lens. (b) Calculated dispersion of SPP currents obtained by spatial Fourier transform of near-fields of the SPP currents. A dashed white line indicates the light line in the free-space.

Herein, we demonstrate multiple resonant SPP antenna radiations over a whole visible range by employing a single-crystalline Ag NW and investigate the radiation properties in the Fresnel region. The Ag NWs were synthesized by the vapor transport method at a very high temperature, which provides defect-free crystallinity and atomically smooth surface. The NW minimizes random scattering of SPP and thus establishes very high-quality SPP resonances, thereby clearly displaying unique antenna radiating near-field patterns. The characteristics of the SPP antennas were analyzed quantitatively using antenna theory and full-field electromagnetic simulations. We anticipate that the multiple resonant NW antennas would contribute to deeper fundamental understanding of nanoantenna operation and could find diverse applications in surface-enhanced Raman scattering,[33−36] highly enhanced photodetection,[37−40] photovoltaics,[41,42] high-resolution nanoimaging,[17−20] and nonlinear signal conversion.[43−46]

Single-Crystalline Ag NW SPP Nanoantenna. Single-crystalline Ag NWs were synthesized by simple vapor transport method using a Ag slug as a precursor (Figure S1a of the Supporting Information). Figure 1a shows the scanning electron microscope (SEM) image of as-synthesized Ag NWs. The NWs have round-shaped tips, diameters of 100−200 nm, and lengths of a few or tens of micrometers. Transmission electron microscope

dx.doi.org/10.1021/nl3002414 | *Nano Lett.* 2012, 12, 2331−2336

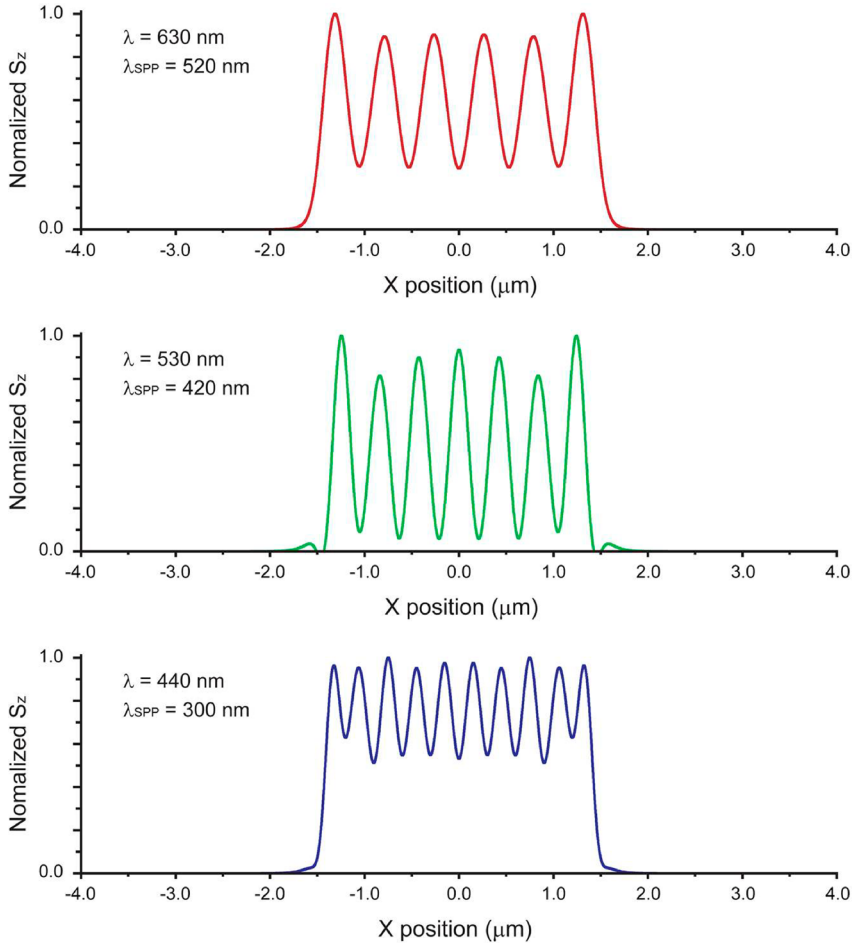

Figure 5. Vertical components of the Poynting vectors were calculated from the vector potential by the SPP currents excited along the NW. The lobes spacing was measured as 295, 410, and 525 nm, where the free-space wavelength and the SPP current wavelength, (λ, λ_{SPP}), are set to be (440, 300), (530, 420), and (630, 520 nm), respectively. The evenly distributed multilobes in the radiating near-field pattern were well-reproduced, as observed in the experiments and the numerical simulations.

(TEM) images and selected area electron diffraction (SAED) patterns of a Ag NW show the single-crystalline nature of NW with atomically smooth surface (Figure S1b,c of the Supporting Information).[47] SPP propagation at a metal/dielectric interface is quite sensitive to the roughness and structural change of the metal surface because surface plasmons exist very close to the interface.[48,49] Moreover, scattering loss gets higher at the shorter wavelength. Because the defect-free Ag NWs have atomically flat and well-defined surfaces whereas nanostructures fabricated by conventional top-down techniques are accompanied by roughness of a few nanometers or more,[29,30,48−50] they are expected to show ideal performances as SPP nanoantennas.[30,49] We also note that Ag has no interband electronic transition in the 430−700 nm spectral range.[26] Consequently, defect-free single-crystal Ag NWs are an ideal material for an optical nanoantenna with a wide spectral range covering all visible and infrared region.

Figure 1b shows a schematic of the antenna radiation from SPPs excited on a single Ag NW. The incident light excites charge-density waves, SPP currents, which propagate back and forth along the NW surface by reflecting at both ends of the NW. The antenna theory predicts that SPP currents propagating toward each other form a standing wave in time-harmonic motion and time-varying currents of charges in a wire create radiations, even if the wire is straight.[1,31,51] Therefore, it is expected that unique multilobe radiation patterns can be generated and observed by SPP standing currents on a Ag NW and in both the Fresnel and Fraunhofer regions.[31,51] Because the charge-density wave is generated along the NW surface, the polarization of the SPP antenna radiation should be parallel to the long axis of NW. The properties of the antenna radiation patterns dominantly depend on the effective index of SPP propagation, the ratio between the SPP propagation wavevector in an NW, and the radiation wavevector in free-space.[1,31,51]

To measure and examine the SPP antenna radiating near-field patterns in the Fresnel region, we placed a single Ag NW onto a glass substrate using a home-built nanomanipulator consisting of a tungsten tip (~100 nm diameter at the end) mounted on a three-axes piezoelectric stage.[52] Figure 1c shows a schematic of the experimental setup to excite the SPP antenna modes and measure their radiation properties at the image plane of the microscope. A laser or white light was injected into the Ag NW at an angle of 80° with respect to the normal direction of glass substrate. The SPP antenna radiating near-field patterns was observed through a dry ×100 objective with a numerical aperture of 0.7 and a charge-coupled device (CCD) camera. Because the incident angle of light is greater than the angle of the numerical aperture, this measurement setup makes up an environment of a dark-field optical microscope, enabling the detection of only SPP antenna radiation separated from the

dx.doi.org/10.1021/nl3002414 | Nano Lett. 2012, 12, 2331−2336

direct reflection by the substrate. A linear polarizer in front of the CCD camera determined the polarization states of the antenna radiations.

SPP Nanoantenna Operation of a Ag NW in the Full Visible Range. To investigate the operation wavelength range of single-crystalline Ag NW, we employed three different color laser sources with wavelengths of 440 (blue), 532 (green), and 633 nm (red). The three figures at the top of Figure 2a are radiating near-field patterns excited by these three lasers when the polarizer was set to detect only the light polarized parallel to the NW, and the three figures at the bottom detect only the light polarized perpendicular to the NW. An optical micrograph of the investigated Ag NW with a length of 3.1 μm and a diameter of 150 nm is also shown at the top of Figure 2a. At all three wavelengths, we clearly observed unique antenna radiation patterns of multilobes in the Fresnel region. The parallel polarization of antenna radiations to the NW strongly indicates that they originated from the SPP currents on the Ag NW. The incident laser has parallel polarization to the incident plane, which can reduce light reflection from the substrate more than perpendicular polarization at an angle moderately greater than the Brewster angle, improving the visibility of SPP antenna radiation against a background noise. The angle between the incident laser beam and the NW axis (θ in Figure 1c) was set to ~60° to make sure that the incident electric fields have both parallel and perpendicular components with respect to the NW axis.

We found that the spacing of the lobes increases as the excitation laser wavelength increases, measured as ~420 (blue), 510 (green), and 600 (red) nm, respectively. The lobe spacings are shorter than the free-space light wavelengths, reflecting the sub-wavelength-scale properties of the SPP antenna modes. Notably, the single-crystalline Ag NW, with its atomically flat surface, extended reliable SPP antenna operation to the blue wavelength, demonstrating an optical nanoantenna operating in the full visible range. In general, the shorter wavelength SPP supports the smaller mode volume and the higher field confinement.

The lobe spacing in the radiating near-field pattern provides valuable clues for the role of SPP currents in generating the antenna radiations. Figure 2b shows that the lobe spacings are independent of θ, indicating that the observed pattern results are from the induced SPP currents, of which wavevector is independent of θ, and not from the diffracted light. Therefore, the single Ag NW acts as a transmitting optical nanoantenna that transduces current signals into outgoing antenna radiations to the free-space.

Rainbow Antenna Radiation from Multiple Resonances. As a 1-D SPP cavity, the Ag NW antenna supports its resonance modes by reflecting SPP currents at both ends of the NW. The propagation wavelength of SPPs in the cavity, λ_{SPP}, are given by the waveguide modes of the NW, which depends on the NW diameter. The resonance condition of a NW antenna is determined by the NW length, which is slightly shifted from the multiples of $\lambda_{SPP}/2$ because the ends of NW are not rigid mirrors.[31,53] In a sufficiently long NW antenna, several resonance modes can exist over the full visible frequency range. When SPP currents are excited by a white light source, distinct conditions for each resonance make radiating near-field lobes appear at different locations of the Ag NW, leading to a colorful radiation pattern like a rainbow (Figure 3a). In this rainbow radiation experiment by the white light, we employed a Ag film prepared by electron beam evaporation instead of a glass substrate to boost the vertical radiation of the NW antenna and enhance the signal-to-noise ratio. The Ag NW antenna is 41 μm long and has a diameter of 180 nm. The propagation length of SPPs in the Ag/air interface is typically from 10 to 100 μm in the visible regime.[54] Because the SPP propagation length of the blue wavelength is shorter than the NW length, we can observe strong radiations of the wavelengths from green to red colors, where SPPs can successfully evolve antenna resonances through the 41 μm long NW. Indeed, the ultrasmooth surface of a very long Ag NW enabled successful operation of multiple SPP antenna resonances with a wide spectral range (Figure S2 of the Supporting Information).

Discussion. To investigate further antenna radiations from the excited SPP currents in the Fresnel region and examine the experimental results, we performed full-field electromagnetic simulations based on the finite-difference time-domain (FDTD) method.[55] Figure 4a shows the vertical component distributions of the Poynting vectors of the antenna radiations at different free-space light wavelengths. The diameter and length of a Ag NW were set as the same values of the NW in Figure 2a, and the SPP currents were excited by injecting a plane wave at an incident angle of 80°. We surrounded the Ag NW by air to study the response of the NW antenna. The glass substrate with a low refractive index of ~1.5 mostly influences spectral positions of the antenna resonances rather than their field distributions.[27] The calculated Poynting vector distributions were captured at a plane 150 nm above the NW axis. The calculations clearly reproduced the unique multilobe radiating near-field patterns and showed that their polarization states are parallel to the NW axis.

At incident wavelengths of 440, 530, and 630 nm, the spacings of the lobes were calculated to be about 300, 420, and 520 nm, respectively. These values exactly correspond to λ_{SPP}, as obtained from the dispersion curve of the SPP currents propagating along the Ag NW, plotted in Figure 4b, indicating that the antenna radiation is really originated from SPP currents on the NW. The discrepancies between these theoretically predicted spacings and the experimentally measured values (420, 510, and 600 nm) are due to expansion of the lobes and their spacings in proportion to the distance from the NW to the measurement plane, the focal plane in this experiment. Additionally, the numerical aperture and limited resolution of the objective lens further blur details in the radiating near-field pattern. Considering the experimental limits of the optical measurements in the Fresnel region, such as depth of field, the theoretical calculations reproduce accurately most of the unique experimental features, the radiating near-field pattern, strongly polarized states, and the lobe spacings.

The observed properties of the antenna radiation can be also successfully understood by employing the antenna theory.[1,31] We point out that SPPs propagating on the NW determine the effective surface current by $\vec{K} = \vec{n} \times \vec{H}_{tan}$, where $\vec{n}$ and $\vec{H}_{tan}$ are the surface normal vector and the tangential magnetic field on the surface, respectively. Upon injection of incident light, as shown in Figure 1c, the induced current $\vec{K} = K(x)\hat{x}$ along the x axis consists of two parts: a uniform surface current coming from a direct coupling of light onto the NW surface and a plasmonic current excited at the NW end in the form of a standing wave. Here the NW axis is set as the x axis. As current vanishes at the end of an NW, we have approximately $K(x) \propto \cos(k_{SPP}L/2) - \cos(k_{SPP}x)$ for the NW located in the region $-L/2 \leq x \leq L/2$, where k_{SPP} is the wavenumber of the SPPs.

dx.doi.org/10.1021/nl3002414 | Nano Lett. 2012, 12, 2331−2336

According to the antenna theory, SPP antenna radiation from a Ag NW of length L is determined by the magnetic vector potential as $A_x(x,z) = (\mu/4\pi) \sin\theta \int_{-L/2}^{L/2} K(x')(e^{ikR}/R)\, dx'$. Here k is the wavevector in the free space and $R = (z^2 + (x - x')^2)^{1/2}$ is the distance of the observation point, (x,z), from the position of the SPP current component, $K(x')$. The origin of the coordinate is the center of the NW, and z is the height of the observation point above the NW. Figure 5 displays the vertical component distribution of the Poynting vector based on the vector potential of a 3.1 μm long Ag NW. The antenna theory analysis indicates that the sizable difference between the λ_{SPP} and the free-space wavelength λ is responsible for the evenly spaced radiating near-field pattern, as seen in Figures 2a and 4a (Figure S3 of the Supporting Information). As λ_{SPP}/λ gets smaller than 1, the intensity of major lobe decreases, whereas those of minor lobes remain nearly unchanged.[1,31]

In conclusion, the rainbow radiating near-field pattern observed in the defect-free single-crystalline Ag NW has been fully reproduced and analyzed through antenna theory and numerical FDTD simulations and interpreted as induced by multiple SPP resonances in the NW antenna. The multiple resonant Ag NW antenna would find diverse physical and biochemical applications including high-resolution microscopy[17−20] and sensing.[21−25]

■ ASSOCIATED CONTENT

Supporting Information

Experimental details including synthesis of single-crystalline Ag NWs, measurement of radiating near-field patterns of SPP antenna from the longer Ag NW, FDTD simulations, and antenna theory analysis. This material is available free of charge via the Internet at http://pubs.acs.org.

■ AUTHOR INFORMATION

Corresponding Author

*E-mail: bongsoo@kaist.ac.kr (B.K.); qpark@korea.ac.kr (Q.-H.P); minkyo_seo@kaist.ac.kr (M.-K.S.).

Notes

The authors declare no competing financial interest.

■ ACKNOWLEDGMENTS

We acknowledge support of this work by KI NanoCentury in KAIST (B.K. and M.-K.S.) and NRF grants (B.K.: 2011-0020419, 2012-0000648, 2011-K000210; Q.-H.P.: 2011-0029807, 2011-0019170, 2011-0020205; M.-K.S.: 2011-0015119) funded by MEST.

■ REFERENCES

(1) Balancis, C. A. *Antenna Theory: Analysis and Design*; Wiley: New York, 2005.
(2) Novotny, L.; Hecht, B. *Principles of Nano-Optics*; Cambridge University: New York, 2006.
(3) P. Bharadwaj, B. D.; Novotny, L. *Adv. Opt. Photonics* **2009**, *1*, 438−483.
(4) Greffet, J. J. *Science* **2005**, *308*, 1561−1562.
(5) Muhlschlegel, P.; Eisler, H. J.; Martin, O. J. F.; Hecht, B.; Pohl, D. W. *Science* **2005**, *308*, 1607−1609.
(6) Park, Q.-H. *Contemp. Phys.* **2009**, *50*, 407−423.
(7) Schuller, J. A.; Barnard, E. S.; Cai, W. S.; Jun, Y. C.; White, J. S.; Brongersma, M. L. *Nat. Mater.* **2010**, *9*, 193−204.
(8) Novotny, L.; van Hulst, N. *Nat. Photonics.* **2011**, *5*, 83−90.
(9) Jun, Y. C.; Huang, K. C. Y.; Brongersma, M. L. *Nat. Commun.* **2011**, *2*, 283.
(10) Curto, A. G.; Volpe, G.; Taminiau, T. H.; Kreuzer, M. P.; Quidant, R.; van Hulst, N. F. *Science* **2010**, *329*, 930−933.
(11) Kinkhabwala, A.; Yu, Z. F.; Fan, S. H.; Avlasevich, Y.; Mullen, K.; Moerner, W. E. *Nat. Photonics* **2009**, *3*, 654−657.
(12) Anker, J. N.; Hall, W. P.; Lyandres, O.; Shah, N. C.; Zhao, J.; Van Duyne, R. P. *Nat. Mater.* **2008**, *7*, 442−453.
(13) Taminiau, T. H.; Stefani, F. D.; Segerink, F. B.; Van Hulst, N. F. *Nat. Photonics* **2008**, *2*, 234−237.
(14) Tam, F.; Goodrich, G. P.; Johnson, B. R.; Halas, N. J. *Nano Lett.* **2007**, *7*, 496−501.
(15) Farahani, J. N.; Pohl, D. W.; Eisler, H. J.; Hecht, B. *Phys. Rev. Lett.* **2005**, *95*, 017402.
(16) Kuhn, S.; Hakanson, U.; Rogobete, L.; Sandoghdar, V. *Phys. Rev. Lett.* **2006**, *97*, 017402.
(17) Kalkbrenner, T.; Hakanson, U.; Schadle, A.; Burger, S.; Henkel, C.; Sandoghdar, V. *Phys. Rev. Lett.* **2005**, *95*, 200801.
(18) Novotny, L.; Stranick, S. J. *Annu. Rev. Phys. Chem.* **2006**, *57*, 303−331.
(19) Novotny, L. *Phys. Rev. Lett.* **2007**, *98*, 266802.
(20) Hartschuh, A. *Angew. Chem., Int. Ed.* **2008**, *47*, 8178−8191.
(21) Ha, T.; Enderle, T.; Ogletree, D. F.; Chemla, D. S.; Selvin, P. R.; Weiss, S. *Proc. Natl. Acad. Sci. U.S.A.* **1996**, *93*, 6264−6268.
(22) Lee, J.; Lee, S.; Ragunathan, K.; Joo, C.; Ha, T.; Hohng, S. *Angew. Chem., Int. Ed.* **2010**, *49*, 9922−9925.
(23) Bruchez, M.; Moronne, M.; Gin, P.; Weiss, S.; Alivisatos, A. P. *Science* **1998**, *281*, 2013−2016.
(24) Han, M. Y.; Gao, X. H.; Su, J. Z.; Nie, S. *Nat. Biotechnol.* **2001**, *19*, 631−635.
(25) Somers, R. C.; Bawendi, M. G.; Nocera, D. G. *Chem. Soc. Rev.* **2007**, *36*, 579−591.
(26) Johnson, P. B.; Christy, R. W. *Phys. Rev. B* **1972**, *6*, 4370−4379.
(27) Rossouw, D.; Couillard, M.; Vickery, J.; Kumacheva, E.; Botton, G. A. *Nano Lett.* **2011**, *11*, 1499−1504.
(28) Krenn, J. R.; Schider, G.; Rechberger, W.; Lamprecht, B.; Leitner, A.; Aussenegg, F. R.; Weeber, J. C. *Appl. Phys. Lett.* **2000**, *77*, 3379−3381.
(29) Mock, J. J.; Oldenburg, S. J.; Smith, D. R.; Schultz, D. A.; Schultz, S. *Nano Lett.* **2002**, *2*, 465−469.
(30) Ditlbacher, H.; Hohenau, A.; Wagner, D.; Kreibig, U.; Rogers, M.; Hofer, F.; Aussenegg, F. R.; Krenn, J. R. *Phys. Rev. Lett.* **2005**, *95*, 257403.
(31) Taminiau, T. H.; Stefani, F. D.; van Hulst, N. F. *Nano Lett.* **2011**, *11*, 1020−1024.
(32) Li, Z. P.; Hao, F.; Huang, Y. Z.; Fang, Y. R.; Nordlander, P.; Xu, H. X. *Nano Lett.* **2009**, *9*, 4383−4386.
(33) Stockman, M. I.; Shalaev, V. M.; Moskovits, M.; Botet, R.; George, T. F. *Phys. Rev. B* **1992**, *46*, 2821−2830.
(34) Nie, S. M.; Emery, S. R. *Science* **1997**, *275*, 1102−1106.
(35) Hartschuh, A.; Sanchez, E. J.; Xie, X. S.; Novotny, L. *Phys. Rev. Lett.* **2003**, *90*, 095503.
(36) Fromm, D. P.; Sundaramurthy, A.; Kinkhabwala, A.; Schuck, P. J.; Kino, G. S.; Moerner, W. E. *J. Chem. Phys.* **2006**, *124*, 061101.
(37) Grober, R. D.; Schoelkopf, R. J.; Prober, D. E. *Appl. Phys. Lett.* **1997**, *70*, 1354−1356.
(38) Tang, L.; Kocabas, S. E.; Latif, S.; Okyay, A. K.; Ly-Gagnon, D. S.; Saraswat, K. C.; Miller, D. A. B. *Nat. Photonics* **2008**, *2*, 226−229.
(39) Knight, M. W.; Sobhani, H.; Nordlander, P.; Halas, N. J. *Science* **2011**, *332*, 702−704.
(40) Barnard, E. S.; Pala, R. A.; Brongersma, M. L. *Nat. Nanotechnol.* **2011**, *6*, 588−593.
(41) Pala, R. A.; White, J.; Barnard, E.; Liu, J.; Brongersma, M. L. *Adv. Mater.* **2009**, *21*, 3504−3509.
(42) Atwater, H. A.; Polman, A. *Nat. Mater.* **2010**, *9*, 205−213.
(43) Danckwerts, M.; Novotny, L. *Phys. Rev. Lett.* **2007**, *98*, 026104.
(44) Chang, D. E.; Sorensen, A. S.; Demler, E. A.; Lukin, M. D. *Nat. Phys.* **2007**, *3*, 807−812.
(45) Kim, S.; Jin, J. H.; Kim, Y. J.; Park, I. Y.; Kim, Y.; Kim, S. W. *Nature* **2008**, *453*, 757−760.

(46) Cai, W. S.; Vasudev, A. P.; Brongersma, M. L. *Science* **2011**, *333*, 1720−1723.
(47) Mohanty, P.; Yoon, I.; Kang, T.; Seo, K.; Varadwaj, K. S. K.; Choi, W.; Park, Q.-H.; Ahn, J. P.; Suh, Y. D.; Ihee, H.; Kim, B. *J. Am. Chem. Soc.* **2007**, *129*, 9576−9577.
(48) Huang, J. S.; Callegari, V.; Geisler, P.; Bruning, C.; Kern, J.; Prangsma, J. C.; Wu, X. F.; Feichtner, T.; Ziegler, J.; Weinmann, P.; Kamp, M.; Forchel, A.; Biagioni, P.; Sennhauser, U.; Hecht, B. *Nat. Commun.* **2010**, *1*, 150.
(49) Nagpal, P.; Lindquist, N. C.; Oh, S. H.; Norris, D. J. *Science* **2009**, *325*, 594−597.
(50) *Handbook of Microlithography, Micromachining, and Microfabrication*; SPIE-International Society for Optical Engineering: Bellingham, WA, 1997.
(51) Dorfmuller, J.; Vogelgesang, R.; Khunsin, W.; Rockstuhl, C.; Etrich, C.; Kern, K. *Nano Lett.* **2010**, *10*, 3596−3603.
(52) Kang, T.; Yoon, I.; Jeon, K. S.; Choi, W.; Lee, Y.; Seo, K.; Yoo, Y.; Park, Q.-H.; Ihee, H.; Suh, Y. D.; Kim, B. *J. Phys. Chem. C* **2009**, *113*, 7492−7496.
(53) Huang, K. C. Y.; Jun, Y. C.; Seo, M. K.; Brongersma, M. L. *Opt. Express* **2011**, *19*, 19084−19092.
(54) Maier, S. A. *Plasmonics: Fundamentals and Applications*. Springer: New York, 2007.
(55) Taflove, A.; Hagness, S. C. *Computational Electrodynamics: The Finite-Difference Timedomain Method*, 3rd ed.; Artech House: Boston, 2005.